

Mechanical behavior of FRP confined steel tubular columns under impact

Qiangqiang Liu, Ding Zhou, Jun Wang* and Weiqing Liu^a

College of Civil Engineering, Nanjing Tech University, Nanjing 211816, People's Republic of China

(Received December 9, 2016, Revised January 9, 2018, Accepted April 21, 2018)

Abstract. This paper presents experimental and analytical results of fiber reinforced polymer (FRP) confined steel tubular columns under transverse impact loads. Influences of applied impact energy, thickness of FRP jacket and impact position were discussed in detail, and then the impact responses of FRP confined steel tubes were compared with bare steel tubes. The test results revealed that the FRP jacket contributes to prevent outward buckling deformation of steel at the clamped end and inward buckling of steel at the impact position. For the given applied impact energy, specimens wrapped with one layer and three layers of FRP have the lower peak impact loads than those of the bare steel tubes, whereas specimens wrapped with five layers of FRP exhibit the higher peak impact loads. All the FRP confined steel tubular specimens displayed a longer duration time than the bare steel tubes under the same magnitude of impact energy, and the specimen wrapped with one layer of FRP had the longest duration time. In addition, increasing the applied impact energy leads to the increase of peak impact load and duration time, whereas increasing the distance of impact position from the clamped end results in the decrease of peak impact load and the increase of duration time. The dynamic analysis software Abaqus Explicit was used to simulate the mechanical behavior of FRP confined steel tubular columns, and the numerical results agreed well with the test data. Analytical solution for lateral displacement of an equivalent cantilever beam model subjected to impact load was derived out. Comparison of analytical and experimental results shows that the maximum displacement can be precisely predicted by the present theoretical model.

Keywords: FRP; steel tubes; dynamic response; transverse impact; vibration theory

1. Introduction

Steel columns have been extensively used in fender systems to protect vehicles from colliding with bridge piers. The critical issues of the existing steel fender systems include too rigidity to alleviate the vehicle-structure collision loads, vulnerable erosion in harsh environment and inconveniency to rehabilitation. Fiber reinforced polymer (FRP) composites are being explored to provide high strength-to-weight ratio, corrosion resistance and high energy dissipation capabilities. In China, FRP composite anti-collision systems have been applied to more than 100 bridges. The applications show that FRP composites can effectively prolong the duration time of impact and decrease the impact load (Fang *et al.* 2014 and Chen *et al.* 2014). FRP confined steel tubular columns are treated as hybrid structures. The outer FRP jackets can not only protect the steel from corrosion but also prohibit the outward buckling deformation of steel tube, thus enhance the ductility and strength of the columns. These FRP confined steel tubes have been successfully used as innovative bridge piles or used to strengthen the damaged steel structures (Wang *et al.* 2014a).

Initial research in this area focused on the static behavior of steel structures strengthened or confined by

FRP composites (Feng *et al.* 2015, Ozbakkaloglu and Fanggi 2014, Park and Yoo 2015 and Saeed *et al.* 2016). The studies of Teng and Hu (2007), Haedir and Zhao (2011), Haedir *et al.* (2011) and Bhetwal and Yamada (2012) demonstrated that the elephant's foot mode of buckling failure of hollow steel tubes under axial compression and/or flexural can be effectively prevented through FRP confinement. Haedir and Zhao (2012) presented a simplified design model to evaluate the capacity of carbon fiber reinforced polymer (CFRP) -strengthened steel tubular beams subjected to bending. Fawzia *et al.* (2007) investigated the tensile behavior of high strength steel tubes (yield stress of 1350 MPa) strengthened by carbon/epoxy composites. Their test results indicated that the effective bond length for CFRP with fiber modulus of 640 GPa is around 50 mm, compared to 75 mm for CFRP with fiber modulus of 240 GPa. Wang *et al.* (2014c) reported the compressive behavior of concrete filled double skin steel tubular (CFDST) columns confined by GFRP. Their study revealed that FRP jacket can obviously enhance the carrying capacity of stub columns and the hollow section ratio has little influence on the axial stress-strain. Samaaneh *et al.* (2016) investigated the nonlinear behavior of steel-concrete girders strengthened with CFRP. Their numerical results indicated that the thickness of CFRP at negative moment region has significant influence on the adhesive strength and the positive moment capacity of the composite section. Yousefi *et al.* (2017) studied the flexural behavior of notched steel beams strengthened by CFRP strips. Their test results showed that the additional CFRP strips contributed to prevent crack propagation and

*Corresponding author, Professor,
E-mail: wangjun3312@njtech.edu.cn

^a Professor, E-mail: wqliu@njtech.edu.cn

enhance the ductility of the steel beams. In addition, FRP jackets and self-consolidating concrete were used to rehabilitate the steel piles of East Lynn Lake Bridge in U.S. by Constructed Facilities Center of West Virginia University, and the field test results showed that the load carrying capacity was enhanced 10 times higher under static loads and 3 times higher under dynamic loads (Liang *et al.* 2014 and Vijay *et al.* 2014).

Recently, there are increasing research efforts concerning the impact behavior of FRP composite columns, i.e., hollow and concrete filled FRP columns, as well as FRP-steel tubes. Han *et al.* (2011) studied the crushing behaviors and energy absorption efficiency of pultruded glass fiber reinforced polymer (GFRP) tubes wrapped with carbon or glass braid. Their numerical results showed that by using the 1.0 mm glass fiber over-wrap, the energy absorption capacities of the GFRP tubes were increased by 26.8%-37.4%, whereas the energy absorption capacities of the GFRP tubes with 1.0 mm carbon fiber over-wrap were increased by 34.8%-46.0%. Jiang and Chorzepa (2015) reported a FRP fender system composed of FRP boxes filled with rows of octagonal FRP tubes. Their study revealed that FRP fender system can reduce the peak impact loads on barge and bridge pier by 80% and 88%, respectively. Chen *et al.* (2015) investigated the impact performance of concrete-filled FRP steel tubes under lateral impact load. Their test results showed that the specimens wrapped with GFRP composites sustained 17%-38% higher peak impact load than those wrapped with CFRP composites, and the specimen wrapped with a layer of longitudinal CFRP absorbed more energy than the one wrapped with a layer of transverse CFRP (the thickness of a layer is 0.17 mm). Wang *et al.* (2015) conducted the lateral impact experiment on behavior of CFRP-concrete-steel double skin tubular columns. Their test results showed that under the applied impact energy of 0.56 kJ, the peak impact loads of specimens wrapped with two and three layers of CFRP decreased 24.6% and 41.6%, respectively, compared with the one wrapped with one layer of CFRP, whereas increasing the number of CFRP layers had insignificant effects on the lateral residual deformation. Further increasing both the impact energy and CFRP layers would result in the decrease of lateral residual deformation (Wang *et al.* 2015). Xiao and Shen (2012) performed axial impact experiment on CFRP confined concrete-filled steel tube columns, revealing that increasing the wall thickness of steel tube and providing additional transverse confinement by CFRP can effectively alleviate the impact damage, yielding an increase in the impact load. Huang *et al.* (2017) investigated the impact behavior of concrete filled FRP tubes (CFFTs) with steel spiral reinforcement (SR). With the increase of impact energy, the maximum impact load of CFFTs with SR changed insignificant, while the duration of impact load increased slightly (Huang *et al.* 2017). Alam and Fawzia (2015) conducted numerical study on dynamic responses of CFRP confined square hollow steel tubular columns. Their results showed that by increasing the number of CFRP layers from 1 to 5, the permanent lateral and axial displacements decreased 58.5% and 76.3%, respectively, whereas the peak of impact loads had minor

changes.

Although more attention has been attracted to the impact response of FRP composite structures, the impact behavior of FRP confined hollow steel tubes under transverse impact load has received scant attention. With consistently increasing traffic in recent years, vehicular collision on steel fenders has become more of a prevalent issue (Parvin and Brighton 2014). External FRP jackets can enhance both the load carrying capacity and impact resistance of steel columns. This paper focuses on the responses of FRP confined hollow steel tubular columns under transverse impact load. The influences of applied impact energy, thickness of FRP jacket and loading position are discussed, and then the failure mode and energy absorption of FRP confined hollow steel tubes are compared with those of bare steel tubes. In order to simulate the impact behavior of specimens, finite element models are constructed, and the numerical results are compared with the experimental data. Based on the vibration theory of continuous beams, analytical models are developed to predict the dynamic responses of FRP confined steel tubes.

2. Experimental program

2.1 Materials

Cold-formed circular steel tubes were used in constructing the specimens. Standard tensile coupon tests were conducted to measure the material properties of the steel tubes. All the steel coupons displayed a long plastic plateau after yielding. The measured yield stress of steel is 278.5 MPa and the corresponding Young's modulus is 201.9 GPa.

The FRP laminates were applied directly to the pretreated outer surfaces of the steel tubes. E-glass/isophthalic polyester jackets were used to confine the steel tubes. The fibre longitudinal-circumferential volume fraction is taken as 1:1. To determine the material properties of the GFRP, six coupons were tested in accordance with ASTM D3039/D3039M (2014). The average tensile strength of FRP is 290.93 MPa and the corresponding Young's modulus is 29.38 GPa.

2.2 Test specimen

Seven specimens of FRP confined steel tubular columns were prepared to investigate the influence of impact energy, impact position and thickness of FRP jacket on the dynamic response of columns. Moreover, three bare steel tubes were prepared to observe the differences of their impact behavior with FRP confined steel tubular columns.

All test specimens have a steel tube with thickness of 4.5 mm and outer diameter of 140 mm. The height of the specimens is 1050 mm. Each layer of FRP has a thickness of 0.9 mm. Table 1 shows the detail of the test specimens.

2.3 Experimental set-up

A large impact loading test system has been installed in

Advanced Engineering Composites Research Center of Nanjing Tech University, China. The system consists of a vertical drop weight and a horizontal trolley traction impact testing machines. The former machine was used to test the impact behavior of FRP confined steel tubular specimens and bare steel tube specimens. The mass of a drop hammer with an impactor can be varied from 200 kg to 1200 kg by the change of steel weights. In order to apply impact on the specimens, the T-shaped impactor was fabricated with a semicircular nose. The impactor was made from chromium 15 with hardness of 64 HRC and has a mass of 30 kg. Fig. 1(a) shows the detail of vertical impact load test system.

During test, the hammer is raised automatically by the automatic control system. The maximum drop height is 20 m, in which the applied energy can be varied from 1000 J to 230000 J. In this paper, the drop hammer with a mass of 330 kg was used. Three different drop heights (0.7 m, 1.0 m and 1.3 m) were tried on three new specimens, respectively. The maximum applied energy was selected by the estimated failure load for FRP confined steel tubular column specimens.

According to JTG/T D81 (2006), the column of an anti-collision guardrail on highway is placed 750 mm above the ground, in which the distance of the upper fender to the ground is 600 mm. Steel abutment was used to simulate the fixed constraint at the end of the specimens. The impact loads were applied at 550 mm, 600 mm and 650 mm from the abutment, respectively. Each specimen was subjected to one impact at a certain position. The time histories of impact load were recorded by a piezoelectric sensor mounted onto the drop hammer. A laser displacement transducer and an acceleration transducer were used to continuously record the displacement and acceleration responses at the impact position. The test set-up is shown in Fig. 1(b).

3. Results and discussion

3.1 Damage mode

Fig. 2 shows the condition of the FRP confined steel tubular specimens after impact. Crushing of fibers and

Table 1 Summary of test matrix and results

Specimen ^a	Drop height (m)	Incident energy (J)	Peak load of impact P_i (kN)	Duration time (ms)	Maximum displacement (mm)
SF0a-I	0.7	2310	36.26	41.5	31.29
SF0a-II	1	3300	37.63	47.5	48.22
SF0a-III	1.3	4290	45.69	54.0	62.94
SF3a-I	0.7	2310	32.15	49.5	29.72
SF3a-II	1	3300	33.48	52.5	46.52
SF3a-III	1.3	4290	35.80	56.0	61.31
SF1a-II	1	3300	29.68	71.0	48.18
SF5a-II	1	3300	39.01	51.0	45.06
SF3b-II	1	3300	34.25	49.5	39.92
SF3c-II	1	3300	29.70	55.0	56.28

^a In the first column, the first two letters mean steel and FRP, respectively, 0, 1, 3 and 5 mean the layer number of FRP jacket, respectively, *a*, *b* and *c* correspond to the distances between the impact position and the clamped end 600 mm, 550 mm, and 650 mm, respectively, and I, II and III correspond to the incident energies 2310 J, 3300 J and 4290 J, respectively



(a) Impact load test system



(b) Picture of test set-up

Fig. 1 Impact test set-up

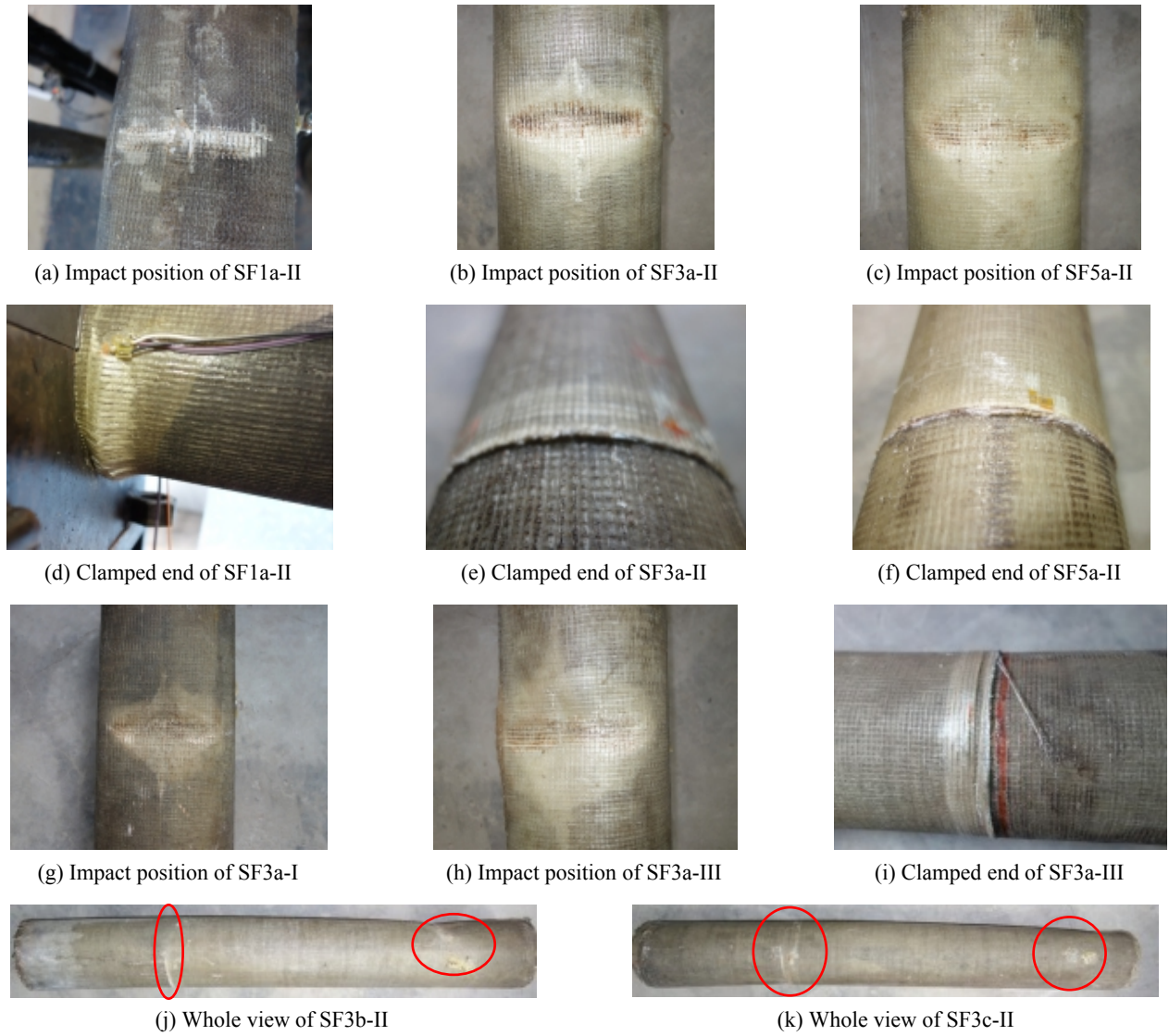


Fig. 2 Typical damage modes of FRP confined steel tubes



Fig. 3 Typical damage modes of steel tubes

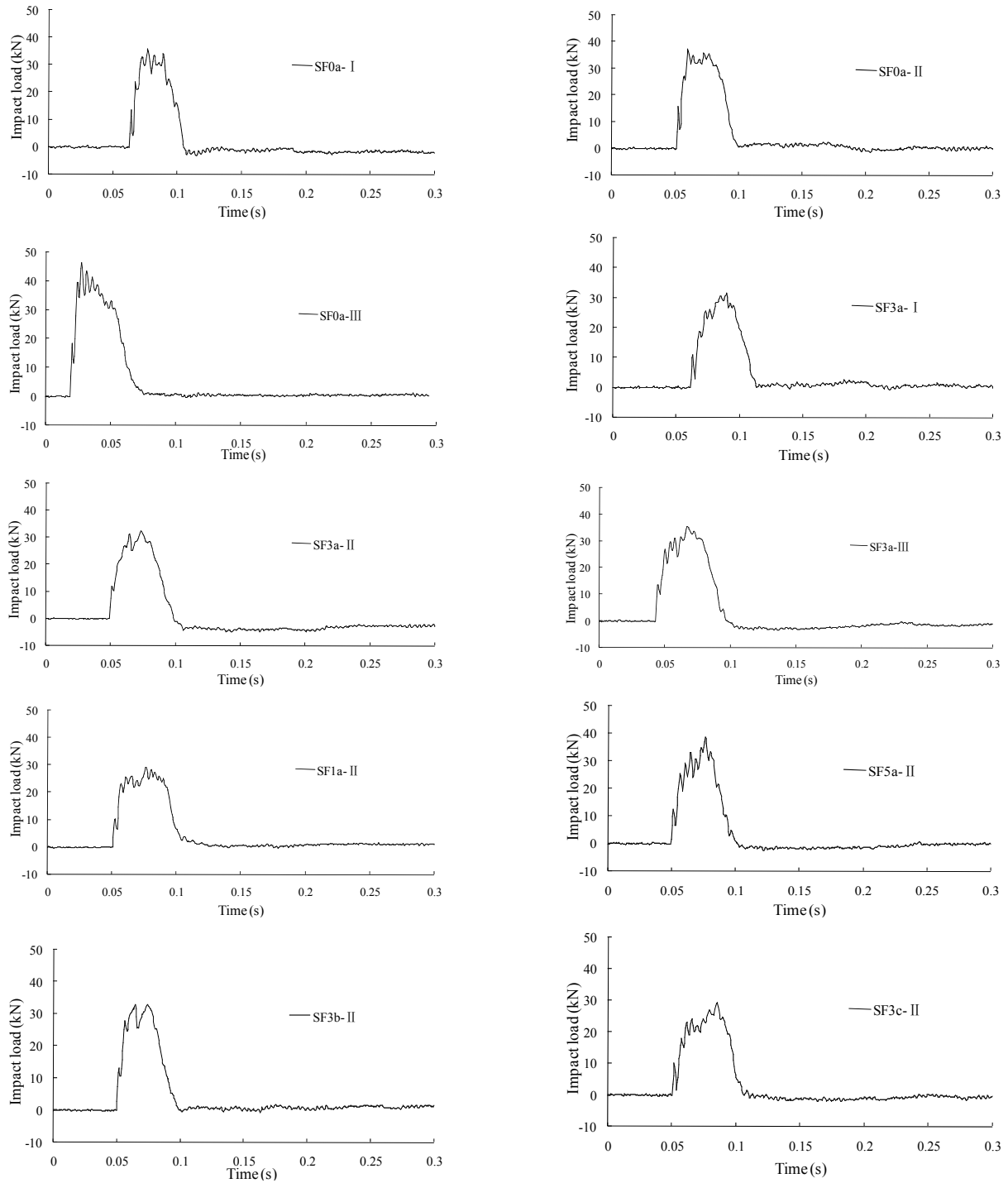


Fig. 4 Impact load-time histories

buckling of the steel wall at the load point were observed for all the specimens wrapped with FRP. Increasing the thickness of FRP jacket can prevent the rupture of fibers at the load point, as shown in Figs. 2(a)-(c). The sections near the clamped end were all damaged to some extents, as shown in Figs. 2(d)-(f). For specimens wrapped with one layer of FRP, elephant's foot buckling of steel was prevalent, resulting in the rupture of FRP due to hoop tension. With the increase in thickness of FRP jacket, the hoop deformation of steel tube near the clamped end was increasingly restrained. For specimens wrapped with two

and three layers of FRP, shear failure of FRP was occurred at the clamped end due to the stress concentration.

With the increase in impact energy, the impact load caused more serious damage both at the impact position and the clamped end, as shown in Figs. 2(g)-(i). However, changing the distance of impact position from the clamped end yields insignificant changes in damage mode, as shown in Figs. 2(j)-(k).

Fig. 3 shows the condition of bare steel tube specimens after impact. Elephant's foot buckling at the clamped end and inward buckling at the load point were occurred for all

the bare steel tube specimens. The increase in impact energy resulted in aggravating the buckling deformation of the steel tube specimens.

3.2 Responses of impact load and acceleration

In general, the impact load-time history curves of specimens wrapped with or without FRP have the similar

shape, as shown in Fig. 4. Firstly, the impact load increased to a peak value in a short time as the specimens were stroked by the impactor. Then, the impact load fluctuated several times due to fast changes of the contact area between the impactor and specimen (Wang *et al.* 2014b). After the specimens and impactor moved downwards together and got the maximum global displacement, they were separated because the impactor rebounded faster than

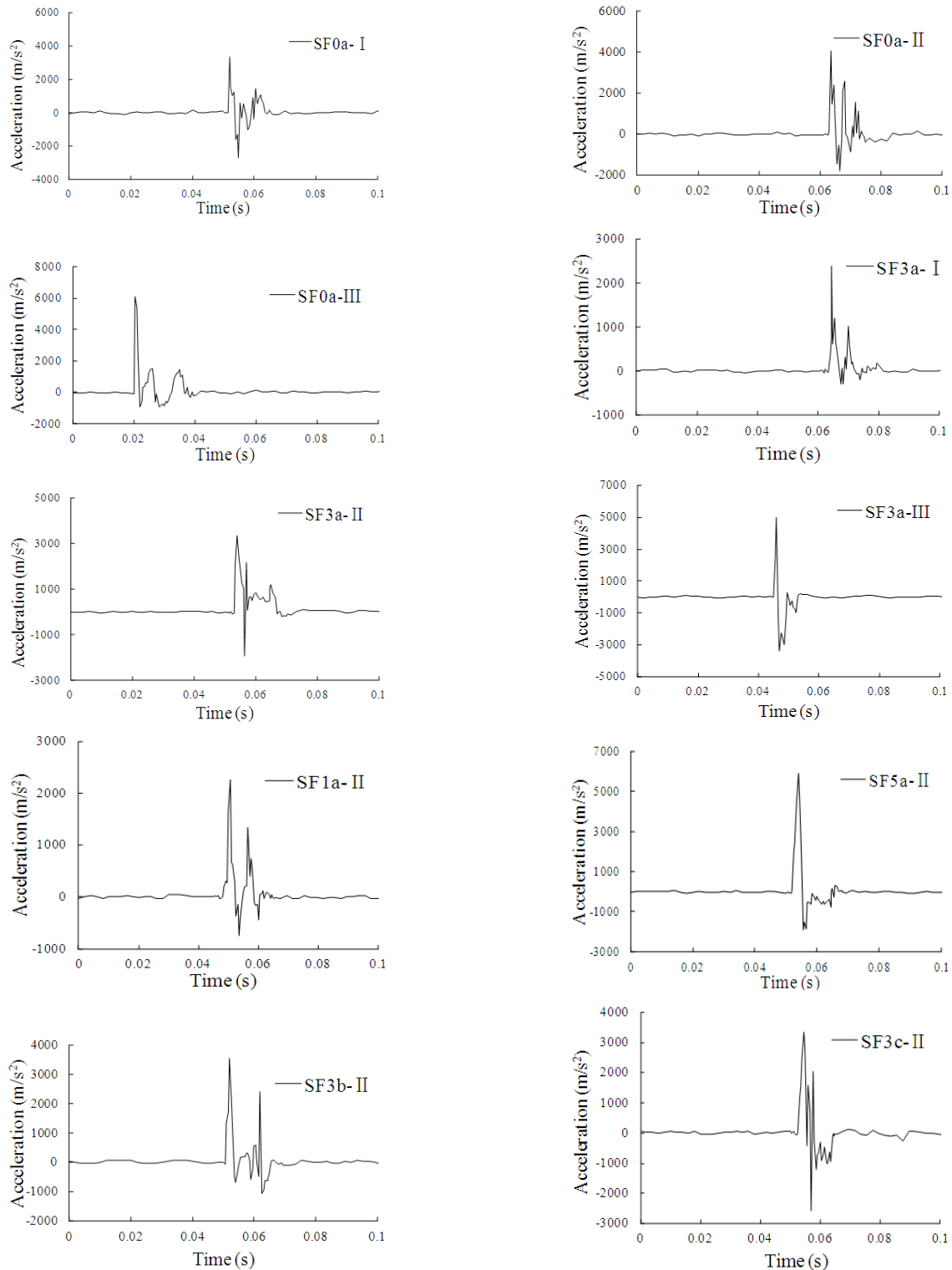


Fig. 5 Acceleration-time histories

the specimens, yielding sudden descending of the impact load. The similar shape of impact load-time histories was also observed in cement filled double steel pipes and CFRP confined concrete-filled steel tubes (Xiao and Shen 2012, Wang *et al.* 2014b).

Under the same applied impact energy, the peak-impact loads of steel tubes wrapped with one or three layers of FRP were lower than those of bare steel tubes, whereas the specimens wrapped with five layers of FRP have higher peak impact loads. In the case of applied impact energy of 3300 J, the peak-impact loads of SF1a-II and SF3a-II decreased 21.23% and 11.03%, respectively, compared with that of SF0a-II, whereas the peak-impact load increased 3.67% for SF5a-II. Similar results were obtained by Chen *et al.* (2015) and Wang *et al.* (2015), in which the peak-impact loads decreased for concrete-filled FRP steel tubes wrapped with one or two layers of FRP and for FRP-concrete-steel double skin tubular specimens wrapped with one to three layers of FRP, compared with those of control specimens (bare steel tubes). Furthermore, the numerical results of Alam and Fawzia (2015) showed that the steel columns strengthened with four or five layers of CFRP had higher peak-impact loads, compared with those of control specimens. Both local stiffness of the impact contact surface and natural frequency of the specimens have significant influences on the peak-impact load (Chen *et al.* 2015). Steel-FRP contact has lower local contact stiffness than steel-steel contact, leading to decreasing the peak-impact load. However, the increase in thickness of FRP jacket can enhance the global stiffness of the specimens, leading to increasing the impact resistance of specimens. Thus, the effects of the thickness of FRP jackets on both the local contact stiffness and global stiffness result in the decrease of peak-impact load for specimens with thin FRP jacket, i.e., one or three layers, as well as the increase of peak-impact load for specimens with thick FRP jacket, i.e., five layers. Similarly, for the given applied impact energy, although the specimens wrapped with FRP had a longer duration time than the bare steel tube specimens, the duration time decreased with the increase of FRP layer numbers. Under the applied impact energy of 3300 J, the duration time of specimens wrapped with one, three and five layers of FRP increased 49.47%, 10.53% and 7.37% respectively, compared to the bare steel tube specimens. In addition, increasing applied impact energy resulted in the increase of peak-impact load, whereas increasing the distance between the load point and the clamped end had a reverse effect.

Acceleration transducers were mounted on each specimen to check the impact load history. Fig. 5 shows the acceleration histories of the tested specimens. Under the same applied impact energy, the peak acceleration of specimens SF0a-II, SF1a-II, SF3a-II and SF5a-II were 4018 m/s², 2263 m/s², 3348 m/s² and 3533 m/s², respectively, indicating that the peak acceleration of the specimens has a trend similar to the peak impact load and duration time. The specimens wrapped with FRP demonstrated lower peak acceleration than the bare steel tubes under the same applied impact energy. Specimen wrapped with one layer of FRP had the lowest peak acceleration in the tested

specimens, and then increasing the number of FRP layers resulted in the decrease in peak acceleration.

3.3 Response of displacement

The displacement histories at the load point were recorded, as shown in Fig. 6, in which the downward displacement was denoted positive. All the specimens showed an initial increase in displacement subjected to impact. After the maximum value was reached, the displacement decreased with the rebound of the specimens, and there was a slight oscillation in displacement. Then, the specimens started to vibrate freely. Finally, the specimens stabilized at a new equilibrium position due to the unrecovered residual deformation.

The maximum displacements at the measured points were shown in Table 1. It can be seen that higher applied impact energy results in higher maximum displacements in test specimens. When the applied impact energy increased from 2310 J to 3300 J and 4290 J, the maximum displacement increased 54.11% and 101.15% for the bare steel tube specimens, respectively, and increased 56.53% and 106.29% for the steel tube specimens wrapped with 3 layers of FRP, respectively. FRP jackets contribute to a slightly decrease in displacements of steel tubes under the same applied impact energy. The maximum displacements of FRP confined steel tubes decreased up to 6.55% compared with those of bare steel tubes. Moving the loading position from *b* to *a* and *c* yielded 16.53% and 40.98% increases in maximum displacements, respectively.

4. Finite element simulation

To provide more comprehensive understanding on the impact responses of steel tubes wrapped with or without FRP, a three dimension FE model has been developed using Abaqus Explicit. The numerical results were compared with those obtained experimentally.

4.1 Material models

The material properties of both FRP and steel were obtained from coupon test results. Elastic model and Hashin failure criteria were used to simulate the brittle rupture of FRP under impact (Hashin 1980). Hashin failure criteria has been successfully applied to predict the impact responses and static behavior of FRP strengthened steel members by Lesani *et al.* (2013), Xie *et al.* (2014), Alam and Fawzia (2015) and Su *et al.* (2016). The material property of steel tube was specified in the elastic-plastic model, in which the plasticity modulus was taken as 50% of elastic modulus. The hammer was made of high strength steel, so it was modeled as a rigid object with a mass of 330 kg and modulus of 201 GPa.

4.2 Construction of model

The 8-node linear brick element with reduced integration and hour-glass control (C3D8R) was used to

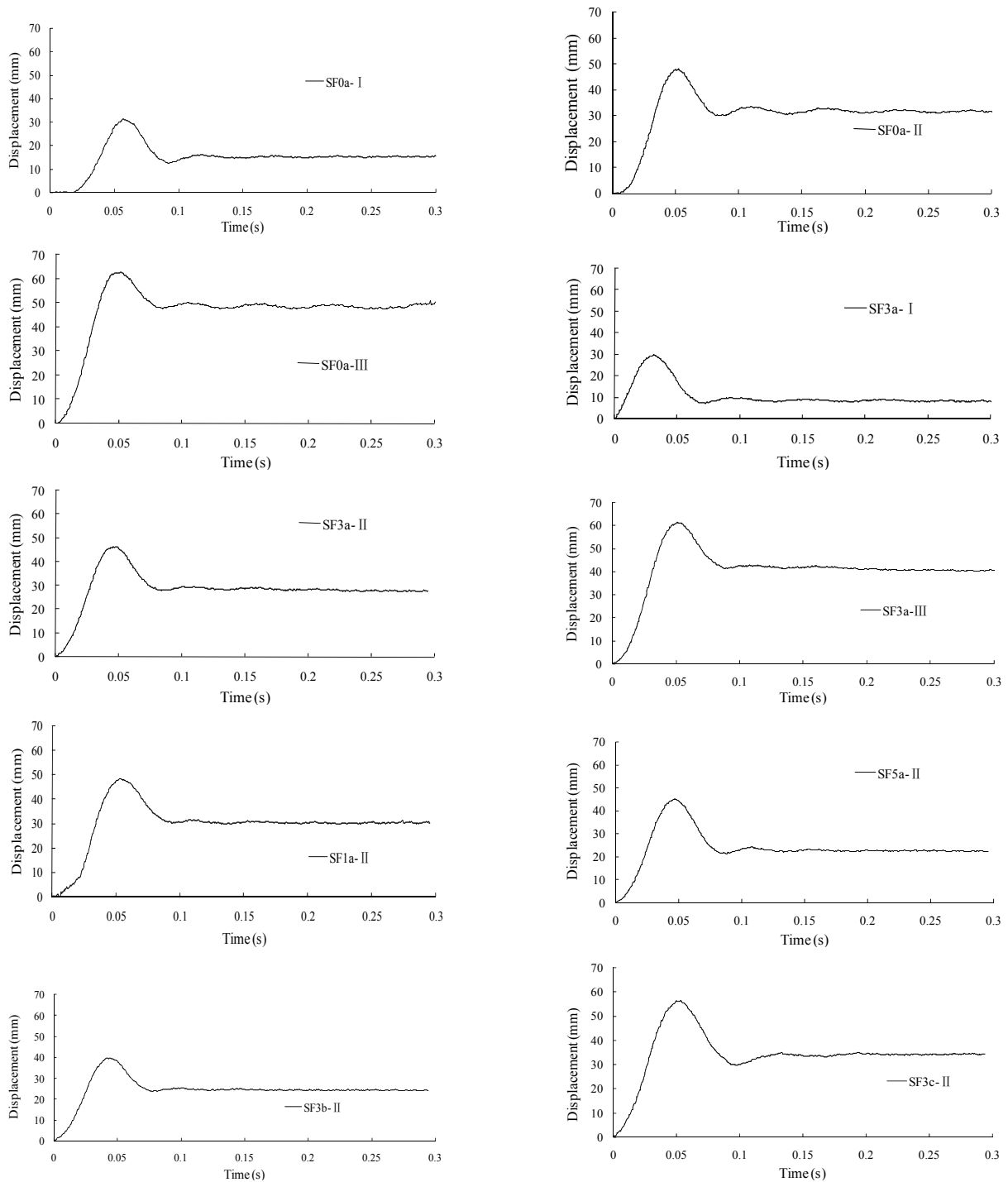


Fig. 6 Displacement-time histories

model the FRP jacket, steel tube and impactor. One end of the test specimen was assumed to be fixed, thus all degrees of freedom at this location were constrained, and the other end was free. The specimens were impacted by the hammer with certain initial velocities. Surface-to-surface contact elements were used to simulate the interface between the impactor and FRP jacket, and even steel tube and FRP jacket. This type of contact is suitable to model load transfer mechanism between the impactor and the specimens (Alam and Fawzia 2015). Moreover, slip and separation that occur between master and slave contact pairs

are considered in surface-to-surface contact. The friction coefficient was taken as 0.3 for the contact surface of steel impactor and steel tube and 0.22 for the contact surface of FRP and steel impactor/tube, respectively (Jiang and Chorzepa 2015).

4.3 Comparison between the numerical values and experimental results

The damage modes of simulated specimens SF0a-II and SF5a-II are shown in Fig. 7. It can be seen in Fig. 7 that the

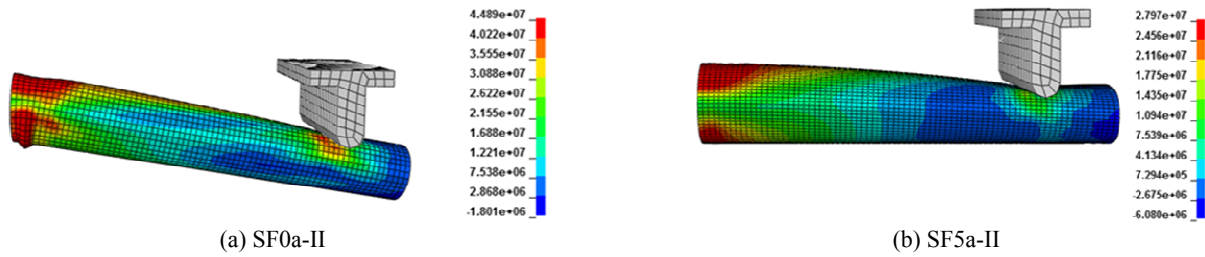


Fig. 7 Simulated specimens

Table 2 Comparison of the peak impact loads between simulated and experimental results

Specimen	Simulated peak impact load (kN)	Tested peak impact load (kN)	δ_1^a
SF0a-I	37.92	36.26	1.05
SF0a-II	40.45	37.63	1.07
SF0a-III	46.56	45.69	1.02
SF3a-I	34.24	32.15	1.07
SF3a-II	35.69	33.48	1.07
SF3a-III	38.24	35.80	1.07
SF1a-II	30.75	29.68	1.04
SF5a-II	42.37	39.01	1.09
SF3b-II	36.06	34.25	1.05
SF3c-II	32.59	29.70	1.09

^a δ_1 is the ratio of simulated peak load to the tested load

developed FE model accurately reproduces the damage modes of steel tube specimens wrapped with and without FRP under impact. The maximum von-Mises stress of bare steel tube specimens occurred simultaneously at the clamped end and the loading area, resulting in elephant's foot buckling of steel at the clamped end and inward buckling of steel at the loading area. For specimens wrapped with 5 layers of FRP, the maximum von-Mises stress occurred at the clamped end, whereas elephant's foot buckling of steel was significantly prevented due to the confinement of FRP jacket.

The simulated and select experimental impact load-time histories of steel tubes wrapped with or without FRP are shown in Fig. 8. The simulated curves in Fig. 8 show that the model offers reasonable trend with the test data, with the FE analyses being capable of capturing the overall shapes of the tested impact load-time histories. Table 2 shows the comparison results of the peak impact loads

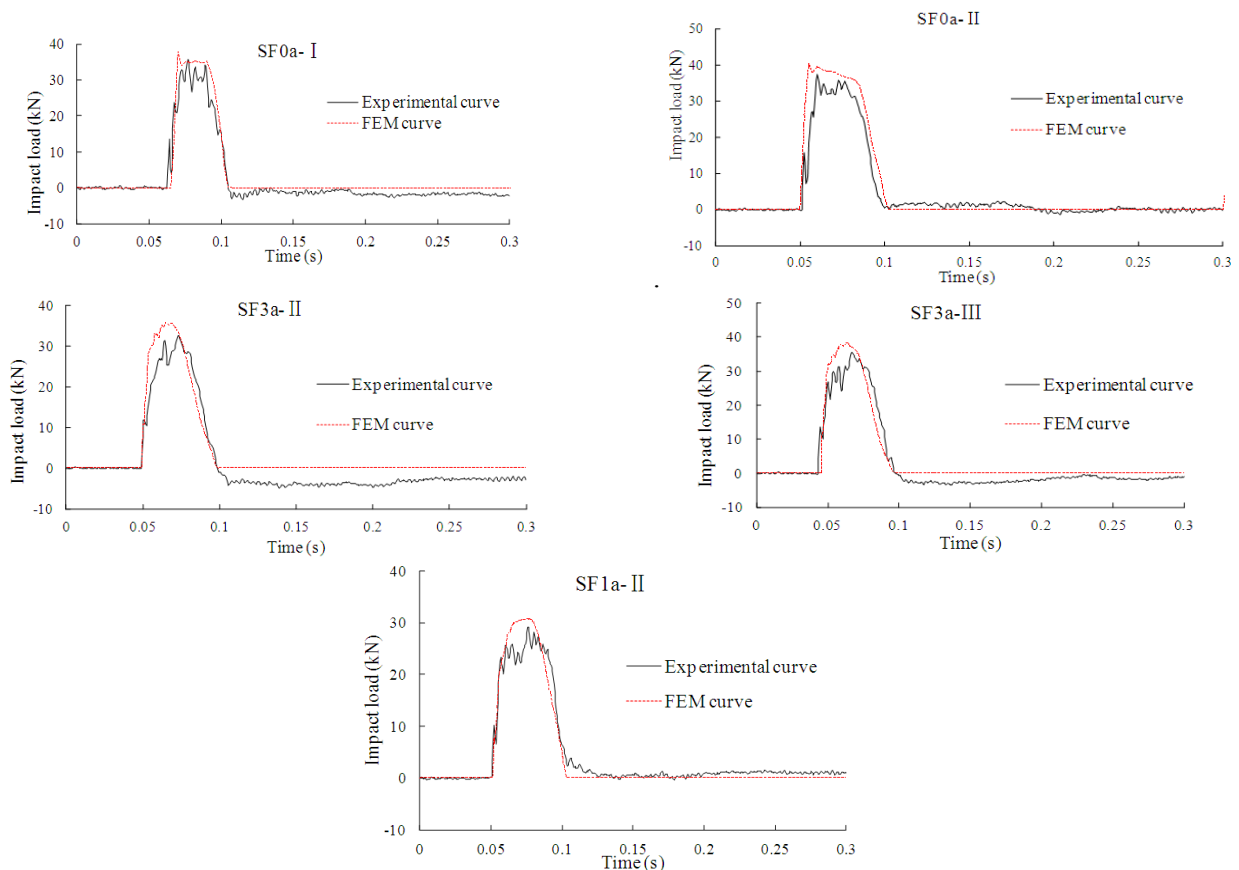


Fig. 8 Comparison of simulated and experimental impact load-time histories

between simulated and experimental results. Results from the FEM are found to be in good agreement with the experimental data.

5. Analytical model of the responses

5.1 Method of analysis

In the derivation of the responses of a continuous beam under transverse impact, the beam is assumed to be longitudinally inextensible and follow the Euler–Bernoulli beam theory where shear deformation and rotary inertia terms are negligible. The boundary conditions are considered to be clamped-free.

The differential equation for lateral displacement of a uniform cantilever beam under impact is shown as (Alper and Daniel 2011)

$$m \frac{\partial^2 V(x,t)}{\partial t^2} + C \frac{\partial V(x,t)}{\partial t} + EI \frac{\partial^4 V(x,t)}{\partial t^4} = F(x,t) \quad (1)$$

where $V(x, t)$ is the lateral displacement, m is the mass of the beam per unit length, C is the damping intensity of the beam, E is the Young's modulus of the materials, I is the inertia of the cross section and $F(x, t)$ is the impact function.

$V(x, t)$ can be considered as a sum of a series of products of spatial functions of only x and time-dependent functions as

$$V(x,t) = \sum_{i=1}^{\infty} \phi_i(x) v_i(t) \quad (2)$$

where $\phi_i(x)$ are the eigenfunctions of a linear uniform cantilever beam and $v_i(t)$ are the generalized time-dependent coordinates.

The impact function $F(x, t)$ is assumed as a rectangular shock pulse to account for the impact load with three phases of initial sudden ascending, a relatively stable plateau and the attenuation stage. Considering the Dirac delta function, the impact function can be expressed as follows

$$\left. \begin{aligned} F(x,t) &= f_p \delta(x-c) & (0 \leq t \leq t_0) \\ F(x,t) &= 0 & (t_0 \leq t) \end{aligned} \right\} \quad (3)$$

where f_p and t_0 are the amplitude and duration of the rectangular shock pulse, respectively, δ is the unit pulse function, and c is the distance between the impact position and the clamped end of the beam.

Substituting Eq. (2) into Eq. (1) and multiplying $\phi_j(x)$ to both sides of the Eq. (1) yield

$$\begin{aligned} & \sum_{i,j=1}^{\infty} m \ddot{v}_i(t) \phi_i(x) \phi_j(x) + \sum_{i,j=1}^{\infty} C \dot{v}_i(t) \phi_i(x) \phi_j(x) + \sum_{i,j=1}^{\infty} EI v_i(t) \phi_i(x) \frac{d^4 \phi_j(x)}{dx^4} \\ & = \sum_{j=1}^{\infty} \phi_j(x) F(x,t) \end{aligned} \quad (4)$$

Integrating each term of Eq. (4) over the span l and dividing m from both sides of the Eq. (4) yield

$$\ddot{v}_i(t) + 2\xi_i \omega_i \dot{v}_i(t) + \omega_i^2 v_i(t) = \int_0^l \frac{F(x,t) \phi_i(x)}{m} dx \quad (5)$$

The right side of Eq. (5) can be expressed as in which

$$\xi_i = \frac{C}{2m\omega_i}$$

$$\int_0^l \frac{F(x,t) \phi_i(x)}{m} dx = \int_0^l \frac{\delta(x-c) \phi_i(x) f(t)}{m} dx = \frac{\phi_i(c)}{m} f(t) \quad (6)$$

in which

$$\left. \begin{aligned} f(t) &= f_p & (0 \leq t \leq t_0) \\ f(t) &= 0 & (t_0 \leq t) \end{aligned} \right\} \quad (7)$$

Substituting Eqs. (6)-(7) into Eq. (5), the solution of v_i can be obtained

$$v_i = \phi_i(c) f_p \left[1 - e^{-\xi_i \omega_i t} \left(\cos \omega_i \sqrt{1 - \xi_i^2} t + \frac{\xi_i}{\sqrt{1 - \xi_i^2}} \sin \omega_i \sqrt{1 - \xi_i^2} t \right) \right] \quad (8)$$

($0 \leq t \leq t_0$)

$$\begin{aligned} v_i &= \phi_i(c) f_p \left[-e^{-\xi_i \omega_i t} \left(\cos \omega_i \sqrt{1 - \xi_i^2} t + \frac{\xi_i}{\sqrt{1 - \xi_i^2}} \sin \omega_i \sqrt{1 - \xi_i^2} t \right) \right] \\ &+ \phi_i(c) f_p \left[e^{-\xi_i \omega_i t'} \left(\cos \omega_i \sqrt{1 - \xi_i^2} t' + \frac{\xi_i}{\sqrt{1 - \xi_i^2}} \sin \omega_i \sqrt{1 - \xi_i^2} t' \right) \right] \quad (9) \end{aligned}$$

($t_0 \leq t$)

in which $t' = t - t_0$

The eigenfunction of a uniform cantilever beam with a tip mass M is given as (Alper and Daniel 2011)

$$\phi_i = A_i \left[\cos \frac{\lambda_i}{L} x - \cosh \frac{\lambda_i}{L} x + \beta_i \left(\sin \frac{\lambda_i}{L} x - \sinh \frac{\lambda_i}{L} x \right) \right] \quad (10)$$

where A_i is the modal constant, L is the distance between the tip mass and the clamped end, λ_i is the eigenvalue, and β_i is given by

$$\beta_i = \frac{\sin \lambda_i - \sinh \lambda_i + \lambda_i \frac{M}{mL} (\cos \lambda_i - \cosh \lambda_i)}{\cos \lambda_i + \cosh \lambda_i - \lambda_i \frac{M}{mL} (\sin \lambda_i - \sinh \lambda_i)} \quad (11)$$

The eigenvalue can be obtained from characteristic equation as follow

$$1 + \cos \lambda_i \cosh \lambda_i + \lambda_i \frac{M}{mL} (\cos \lambda_i \sinh \lambda_i - \sin \lambda_i \cosh \lambda_i) = 0 \quad (12)$$

Thus, calculating the eigenvalue from Eq. (12), and then substituting Eqs. (8), (9) and (10) into Eq. (2), the displacement responses of a cantilever beam with a tip mass subjected to transverse impact can be obtained.

5.2 Comparison between theoretical formulas with experimental results

For the tested specimens, the impactor was dropped, and then vibrated with the specimens together. Thus, the tip mass with 330 kg was considered in deriving the responses. The damping ratio was obtained from the logarithmic decrement of displacement responses. f_p was determined by area equivalent method, in which the area under the tested impact curve was assumed to be equal to the rectangular area during the time t_0 . Moreover, only the first three modes were considered to simplify the calculation.

Considering the impact damage of FRP and steel, the bending stiffness of FRP confined steel tube columns EI is given by

$$EI = \alpha E_f I_f + \beta E_s I_s \quad (13)$$

where α and β are the modulus retention ratios of FRP and steel subjected to impact, respectively, E_f and I_f are the Young's modulus and inertial of FRP jacket, respectively, and E_s and I_s are the Young's modulus and inertial of steel tube, respectively.

As mentioned in Cheng *et al.* (2009), the reduced modulus is related to the damage area of FRP laminate. It was found that the value of α was in the range of 0.11 and 0.19, and the compression strength after impact (CAI) was not sensitive to the value from 0.11 to 0.19. Thus, α is taken as 0.15 which is the mean value of 0.11 and 0.19. Moreover, considering the plastic deformation of steel under impact, the plasticity modulus of the steel was used to calculate EI . Thus, β is taken as a value of 0.5 because the plasticity modulus of the steel is assumed 50% of its elastic modulus (Shaat and Fam 2007). For bare steel tube specimens, α is taken as 0.

Eq. (13) was used to calculate the bending stiffness of FRP confined steel tubular specimens and bare steel tube specimens. Comparisons of the analytical and the measured maximum displacements are shown in Table 3. Analytical results of the peak displacement show good agreements with the experimental results.

Table 3 Comparison of the maximum displacements between analytical and experimental results

Specimen	Analytical maximum displacement (mm)	Measured maximum displacement (mm)	δ^a
SF0a-I	30.54	31.29	0.98
SF0a-II	49.71	48.22	1.03
SF0a-III	57.01	62.94	0.91
SF3a-I	27.95	29.72	0.94
SF3a-II	49.96	46.52	1.07
SF3a-III	64.82	61.31	1.06
SF1a-II	43.90	48.18	0.91
SF5a-II	46.50	45.06	1.03
SF3b-II	39.70	39.92	0.99
SF3c-II	60.09	56.28	1.07

^a δ is the ratio of analytical maximum displacement to the measured data

6. Conclusions

To investigate the mechanical behavior of FRP confined steel tubular columns under transverse impact load, a series of impact tests were conducted for the given impact energies (by varying the dropping height), the impact position and the thickness of FRP jackets. The time histories of the impact load, acceleration and displacement response of the specimens were instrumented and theoretically calculated. The results obtained from this study are summarized as follows:

- Elephant's foot buckling at the clamped end and inward buckling at the impact position are the most prevalent damages in the hollow steel tubes, whereas the shear failure of FRP occurs at the clamped end of FRP confined steel tubes. The outward buckling deformation of steel near the clamped and the rupture of fibers at the impact position are remarkably restrained by FRP jackets with 3 or 5 layers. Moreover, with the increase of applied impact energy, more serious damage occurs both at the impact position and at the clamped end. However, the distance between the impact position and the clamped end has insignificant effect on damage mode.
- Compared with bare steel tubes, the specimens wrapped with one or three layers of FRP have lower peak impact load, whereas those wrapped with five layers of FRP result in higher peak impact load. All of FRP confined steel tube specimens show longer duration time than the bare steel specimens under the same applied impact energy. However, the specimen wrapped with one layer of FRP has the longest duration time in FRP confined steel tubular specimens. Steel tubes wrapped with a thin FRP jacket contribute to decrease local stiffness at impactor-column contact surface, whereas the increase in thickness of FRP jacket leads to the enhancement of the global stiffness of the columns. Both the local stiffness at impact surface and the global stiffness of the columns have significant influences on the peak impact load and the duration.
- The dynamic analysis program Abaqus Explicit was used to simulate the impact behaviors of tested specimens. The models provide reasonable simulations of the tested results of impact load-time histories for both bare steel tubes and those wrapped with FRP.
- The dynamic response of a uniform cantilever beam subjected to impact was solved. The bending stiffness which considered the impact damage effects was introduced in the analysis. The present model can perfectly simulate the maximum displacement.

Acknowledgments

The financial supports from National Natural Science Foundation of China (Grant No. 51578283), National Key Basic Research Program of China (973Program, Grant No. 2012CB026205) are highly appreciated.

References

- Alam, M.I. and Fawzia, S. (2015), "Numerical studies on CFRP strengthened steel columns under transverse impact", *Compos. Struct.*, **120**, 428-441.
- Alper, E. and Daniel, J.I. (2011), *Piezoelectric Energy Harvesting, Appendix C: Modal Analysis of a Uniform Cantilever With a Tip Mass*, John Wiley & Sons, New York, NY, USA, pp. 353-356.
- ASTM D3039/D3039M (2014), Standard test method for tensile properties of polymer matrix composite materials, USA.
- Bhetwal, K.K. and Yamada, S. (2012), "Effects of CFRP reinforcements on the buckling behavior of thin-walled steel cylinders under compression", *Int. J. Struct. Stab. Dy.*, **12**(1), 131-151.
- Chen, C.H., Zhu, X., Hou, H., Zhang, L., Shen, X. and Tang, T. (2014), "An experimental study on the ballistic performance of FRP-steel plates completely penetrated by a hemispherical-nosed projectile", *Steel Compos. Struct., Int. J.*, **16**(3), 269-288.
- Chen, C., Zhao, Y. and Li, J. (2015), "Experimental investigation on the impact performance of concrete-filled FRP steel tubes", *J. Eng. Mech.-ASCE*, **141**(2), 197-201.
- Cheng, X., Al-Mansour, A.M. and Li, Z. (2009), "Residual strength of stitched laminates after low velocity impact", *J. Reinf. Plast. Compos.*, **28**(14), 1679-1688.
- Fang, H., Liu, W., Zhuang, Y. and Zhu, L. (2014), *Analysis and Design of Floating Composite Anti-collision Bumper System for Large Bridge*, Research and application of composite materials in Infrastructure, China Architecture & Building Press, pp. 40-47.
- Fawzia, S., Al-Mahaidi, R., Zhao, X.L. and Rizkalla, S. (2007), "Strengthening of circular hollow steel tubular sections using high modulus of CFRP sheets", *Constr. Build. Mater.*, **21**(4), 839-845.
- Feng, P., Cheng, S., Bai, Y. and Ye, L. (2015), "Mechanical behavior of concrete-filled square steel tube with FRP-confined concrete core subjected to axial compression", *Compos. Struct.*, **123**, 312-324.
- Haedir, J. and Zhao, X.L. (2011), "Design of short CFRP-reinforced steel tubular columns", *J. Constr. Steel Res.*, **67**(3), 497-509.
- Haedir, J. and Zhao, X.L. (2012), "Design of CFRP-strengthened steel CHS tubular beams", *J. Constr. Steel Res.*, **72**(4), 203-218.
- Haedir, J., Zhao, X.L., Grzebieta, R.H. and Bambach, M.R. (2011), "Non-linear analysis to predict the moment-curvature response of CFRP-strengthened steel CHS tubular beams", *Thin-Wall. Struct.*, **49**(8), 997-1006.
- Han, H., Taheri, F. and Pegg, N. (2011), "Crushing behaviors and energy absorption efficiency of hybrid pultruded and $\pm 45^\circ$ braided tubes", *Mech. Adv. Mater. Struct.*, **18**(4), 287-300.
- Hashin, Z. (1980), "Failure criteria for unidirectional fiber composites", *J. Appl. Mech.*, **47**(2), 329-334.
- Huang, L., Sun, X., Yan, L. and Kasal, B. (2017), "Impact behavior of concrete columns confined by both GFRP tube and steel spiral reinforcement", *Constr. Build. Mater.*, **131**, 438-448.
- Jiang, H. and Chorzepa, M.G. (2015), "Evaluation of a new FRP fender system for bridge pier protection against vessel collision", *J. Bridge Eng.*, **20**(2), 05014010.
- JTG/T D81 (2006), Guidelines for design of highway safety facilities, China.
- Lesani, M., Bahaari, M. and Shokrieh, M. (2013), "Numerical investigation of FRP-strengthened tubular T-joints under axial compressive loads", *Compos. Struct.*, **100**, 71-78.
- Liang, R., Skidmore, M. and Ganga Rao, H.V.S. (2014), "Rehabilitation of east lynn lake bridge steel pile bents with composites", *TRB Innovative Technologies for a Resilient Marine Transportation System 3rd Biennial Research and Development Conference*, Washington, DC, USA, June.
- Ozbakkaloglu, T. and Fanggi, B.L. (2014), "Axial compressive behavior of FRP-concrete-steel double-skin tubular columns made of normal- and high-strength concrete", *J. Compos. Constr.*, **18**(1), 04013027.
- Park, J.W. and Yoo, J.H. (2015), "Flexural and compression behavior for steel structures strengthened with Carbon Fiber Reinforced Polymers (CFRPs) sheet", *Steel Compos. Struct., Int. J.*, **19**(2), 441-465.
- Parvin, A. and Brighton, D. (2014), "FRP composites strengthening of concrete columns under various loading conditions", *Polymers*, **6**(4), 1040-1056.
- Saeed, M.S., Majid, B., Hossein, G. and Masood, F. (2016), "Retrofitting of steel pile-abutment connections of integral bridges using CFRP", *Struct. Eng. Mech., Int. J.*, **59**(2), 209-226.
- Samaaneh, M.A., Sharif, A.M., Baluch, M.H. and Azad, A.K. (2016), "Numerical investigation of continuous composite girders strengthened with CFRP", *Steel Compos. Struct., Int. J.*, **21**(6), 1307-1326.
- Shaah, A. and Fam, A. (2007), "Finite element analysis of slender HSS columns strengthened with high modulus composites", *Steel Compos. Struct., Int. J.*, **7**(1), 19-34.
- Su, L., Li, X. and Wang, Y. (2016), "Experimental study and modeling of CFRP-confined damaged and undamaged square RC columns under cyclic loading", *Steel Compos. Struct., Int. J.*, **21**(2), 411-427.
- Teng, J.G. and Hu, Y.M. (2007), "Behaviour of FRP-jacketed circular steel tubes and cylindrical shells under axial compression", *Constr. Build. Mater.*, **21**(4), 827-838.
- Vijay, P.V., Clarkson, J.D., Ganga Rao, H.V.S., Soti, P.R. and Lampo, R. (2014), *FRP Composites for Rehabilitation of Hydraulic Structures*, Research and application of composite materials in Infrastructure, China Architecture & Building Press, pp. 164-171.
- Wang, J., Liu, W., Liang, R. and Ganga Rao, H. (2014a), *Behavior of Concrete and Steel Columns Wrapped with FRP Composites*, Research and application of composite materials in Infrastructure, China Architecture & Building Press, pp. 187-200.
- Wang, Y., Qian, X., Liew, J.Y.R. and Zhang, M.H. (2014b), "Experimental behavior of cement filled pipe-in-pipe composite structures under transverse impact", *Int. J. Impact Eng.*, **72**(4), 1-16.
- Wang, J., Liu, W., Zhou, D., Zhu, L. and Fang, H. (2014c), "Mechanical behaviour of concrete filled double skin steel tubular stub columns confined by FRP under axial compression", *Steel Compos. Struct., Int. J.*, **17**(4), 431-452.
- Wang, R., Han, L.H. and Tao, Z. (2015), "Behavior of FRP-concrete-steel double skin tubular members under lateral impact: experimental study", *Thin-Wall. Struct.*, **95**, 363-373.
- Xiao, Y. and Shen, Y. (2012), "Impact behaviors of CFT and CFRP confined CFT stub columns", *J. Compos. Constr.*, **16**(6), 662-670.
- Xie, Z., Yan, Q. and Li, X. (2014), "Investigation on low velocity impact on a foam core composite sandwich panel", *Steel Compos. Struct., Int. J.*, **17**(2), 159-172.
- Yousefi, O., Narmashiri, K. and Ghaemdoost, M.R. (2017), "Structural behaviors of notched steel beams strengthened using CFRP strips", *Steel Compos. Struct., Int. J.*, **25**(1), 35-43.